2219铝合金搅拌摩擦焊温度场的三维实体耦合数值模拟

杜岩峰[1,2]， 白景彬[1]， 田志杰[1]， 李劲松[1]， 张彦华[2]
(1. 首都航天机械公司，北京 100076; 2. 北京航空航天大学 机械工程及自动化学院，北京 100191)

摘 要: 为更贴近实际的模拟搅拌摩擦焊焊接过程中复杂的热力行为，试验通过建立三维搅拌摩擦焊过程数学模型，采用三维实体耦合的有限元方法来分析2219铝合金搅拌摩擦焊热过程和温度场分布. 结果表明，搅拌摩擦焊焊缝的温度场梯度呈现上密下疏，前密后疏的分布状态，最高温度位于后退侧的搅拌针与轴肩的过渡区，焊缝后退边的温度高于前进边，搅拌针底部温度超过2219铝合金的再结晶温度，可确保对接接头根部形成紧密焊缝，模拟结果为研究搅拌摩擦焊的机理和优化搅拌摩擦焊焊接工艺提供了支持.

关键词: 2219铝合金; 搅拌摩擦焊; 温度场; 数值模拟
中图分类号: TG 453 **文献标识码**: A **文章编号**: 0253-360X(2014)08-0057-04

0 序 言

搅拌摩擦焊过程中，机械能通过搅拌头与被焊材料局部的剧烈摩擦转换为高度集中的热能，焊缝的成形关键在于搅拌针前端要形成具有足够高的温度和足够大的温度梯度，使与搅拌头接触的材料形成粘塑性层[1]，进而在搅拌头的带动下粘塑性层发生流动迁移，过渡到搅拌针后端形成焊缝. 搅拌摩擦焊过程中复杂的热力行为对焊缝成形和质量影响很大. 焊接过程中温度场的建立以及塑性金属的流动与材料的热物理性能、搅拌头、焊接工艺参数、传热条件等密切相关，实时测量焊接温度场分布非常困难，应用数值模拟对搅拌摩擦焊热力过程进行预测分析成为搅拌摩擦焊工艺研究的重要手段[2-6].

在进行搅拌摩擦焊热力过程时需要考虑材料的速率敏感性以及塑性变形与传热的耦合分析，这被称之为热粘塑性耦合分析. 但是由于搅拌摩擦焊局部极端热力行为，使得现有模拟分析中很难考虑搅拌头实体接触摩擦的热力作用，导致模拟结果不能很好反映实际焊接情况. 根据搅拌摩擦焊的物理机制，应用Deform-3D软件实现了2219铝合金搅拌摩擦焊三维温度场的实体全耦合数值模拟，建立三维搅拌摩擦焊过程的数学模型，分析2219铝合金搅拌摩擦焊过程的热过程及温度分布，试验结果可为研究搅拌摩擦焊机理和优化搅拌摩擦焊工艺提供支持.

收稿日期: 2014-03-20

1 搅拌摩擦焊热力耦合模型建立

1.1 几何模型

建立三维实体模型是搅拌摩擦焊热过程实体全耦合数值模拟的基础. 由于Deform-3D本身不具备三维造型的功能，因此实体模型是在三维软件Solidworks中完成，如图1所示.

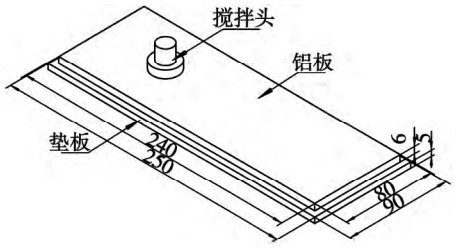

图1 在Solidworks中建立的搅拌摩擦焊物理模型(mm)
Fig. 1 Physical model of friction stir welding established by use of Solidworks

被焊板材为2219铝合金，规格为240 mm×80 mm×6 mm; 垫板采用45钢，规格为250 mm×90 mm×5 mm; 搅拌头外形尺寸为轴肩直径24 mm，内凹角度7°，搅拌针长度5.75 mm，锥角为20°，大端直径5.67 mm，如图2所示.

1.2 网格划分

在Deform-3D软件中可以通过窗口对对象进行网格划分[6]，为更好的模拟搅拌摩擦焊过程中材料的流动，同时有效的降低计算量，提高运行效率，仅

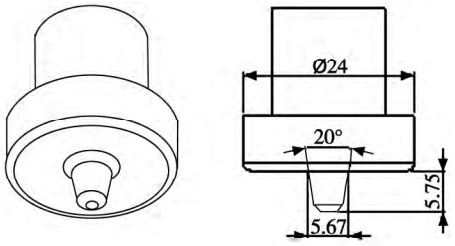

图2 搅拌头的外形尺寸(mm)

Fig. 2 Size of stir-head

将搅拌头与铝板有效作用的区域进行局域网格细化,然后逐渐放大,单元边长从0.5 mm一直过渡到最大6 mm,整个区域由4边体单元组成,共计生成43 300个体单元,节点个数为10 197个,表面几何单元为10 996个. 在移动过程中,设置局部细化网格的区域与焊接速度相同的方向和数值,确保在模拟过程中接触区域的网格比较细化,以期更准确的模拟搅拌摩擦焊的焊缝的成形及热力过程.

搅拌头单元边长从0.3 mm过渡到3 mm,共计生成60 578个体单元,13 807个节点,13 396个表面几何单元. 垫板由于只进行传导热的模拟过程,因此单元尺寸设置比较大,从2.5 mm过渡到5 mm,共计生成17 160个体单元,4 476个节点,5 968个表面几何单元.

1.3 材料模型

在搅拌摩擦焊物理模型中,将搅拌头和垫板均设置成刚性体. 被焊铝板局部区域发生了非常大的塑性变形的粘性流动,其弹性变形量相对于塑性变形量非常小,可以忽略不计,因此在模型中将待焊铝板视为刚(粘)塑性体,其流动应力同时是温度、应变和应变速率的函数. 其它参数不变的情况下,工件温度升高,则同样应变所需的应力减少;应变速率提高,则同样应变所需的应力增加. 2219铝合金的热物理性能考虑温度的影响.

1.4 摩擦系数设定

搅拌摩擦焊过程中的摩擦是在高温发生的,其机制十分复杂,影响因素很多. 为了便于分析计算,通常采用两种简化的摩擦应力模型,即库仑摩擦模型和常应力摩擦模型,分别表示为

$$f=\mu p_n \tag{1}$$

式中:μ 代表库仑摩擦系数,并且 $0<\mu<1$;p_n 为界面的正压力.

常应力摩擦公式为

$$f=m\tau \tag{2}$$

式中:m 为摩擦因子,并且 $0<m\leqslant 1$;τ 为工件材料的剪切屈服应力. 该模型表示,m 给定条件下,摩擦应力 f 与材料的剪切屈服应力 τ 值有关. 当 $m=1$ 时,$f=\tau$,这时接触表面间不产生相对滑动,只是工件材料粘附于模具发生塑性变形.

对于搅拌摩擦焊过程来说,在搅拌头下压阶段,由于系统温度不高,在压力作用下,搅拌针与铝板之间偏向于挤压摩擦,此时宜采用库仑摩擦模型. 随着搅拌针的逐渐压入,铝板的温度升高,尤其是搅拌头轴肩接触到铝板之后,铝板的温度急剧上升,搅拌头与铝板之间逐步的向剪切摩擦过渡,在稳定阶段,搅拌针与铝板之间会形成一层非常薄的中间层,此时可理解为搅拌头带动极薄的基体金属一起运动,而基体金属距离搅拌头不同距离的位置发生不同程度的剪切摩擦,搅拌头与基体之间宜采用常应力摩擦模型,而摩擦系数 m 设置为1,表明铝板材料粘附于搅拌头发生粘塑性变形. 因此在Deform-3D模拟中设置为混合摩擦.

1.5 初始条件和边界条件设定

搅拌摩擦焊三维实体模型所用坐标如图3所示.

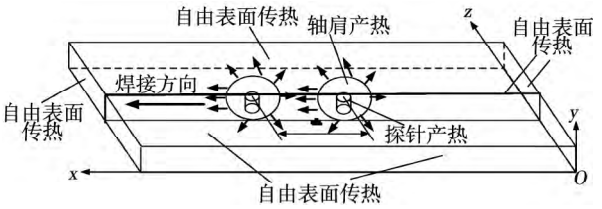

图3 2219铝合金板材的网格划分

Fig. 3 Mesh generation of the plate of 2219 aluminum alloy

初始时,将系统温度定为室温20 ℃,与空气接触的铝板表面属于自由表面,主要为对流换热,边界条件为

$$-k\left.\frac{\partial T}{\partial z}\right|_{y=0}=h_c(T-T_0) \tag{3}$$

式中:h_c 为铝板与环境的对流换热系数,取值为1 N/s·mm·℃;k 为常数;T 为系统温度.

模拟过程中焊接工艺参数设定为下压速度0.2 mm/s,焊接速度120 mm/min,旋转频率800 r/min.

2 搅拌摩擦焊过程温度场模拟及试验结果分析

2.1 搅拌摩擦焊热过程

图4显示的是2219铝合金搅拌摩擦焊从下压开始至焊接结束各个阶段的三维实体温度场的演化过程. 从图4中可以看出,在搅拌头下压的初始阶

段，主要依靠搅拌针与铝合金的接触摩擦产生热量，从前面的分析知道此时搅拌针产生的热量只占总热量比较少的一部分，因此搅拌头下压前期温度场的升高并不快，在搅拌头轴肩与铝板接触之前温度仅达到约 100 ℃，在 $t=25$ s 左右，搅拌头轴肩与铝板初始接触，接触面积显著增大，界面处发生剧烈的摩擦作用，搅拌头所受的摩擦扭矩和下压力也显著增大，摩擦产热急剧升高，接触的铝合金发生了很大的塑性变形，系统的产热机制由摩擦产热逐步向金属塑性变形产热过渡，在 $t=29$ s 时搅拌头下压结束，搅拌头开始行走. 随着焊接的进行，焊接温度迅速升高，并呈放射状向四周扩展，热源周围焊接试件上的温度不断上升. 在焊接刚开始阶段，热源仅使其周围金属的温度上升，而对离热源较远的金属的温度影响不大. $t=41$ s 左右，焊缝区升温开始趋缓，在 $t=57$ s 左右最高温度升到稳定状态的约 410 ℃ 的温度，此后的温度保持小幅的波动，焊接进入了稳定焊接阶段. 当焊接即将结束时，热源到达焊接试件的尾部，热源经过的试件上的温度逐步下降，离搅拌头越远的位置焊缝的温度越低.

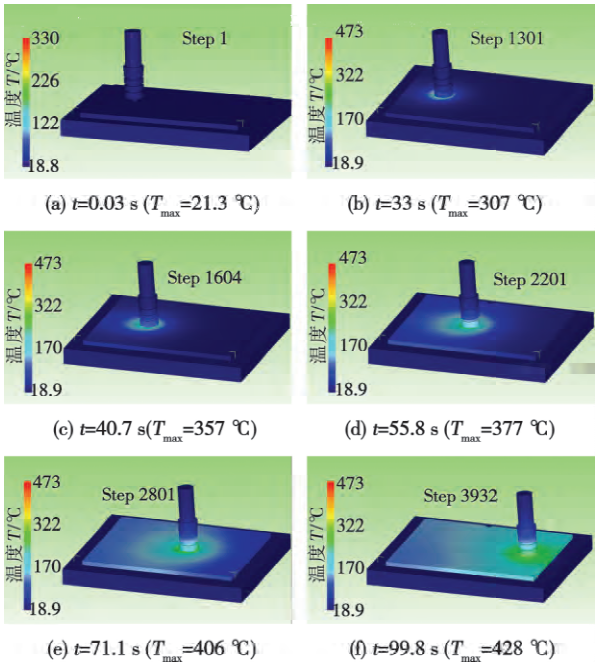

(a) t=0.03 s (T_{max}=21.3 ℃)　(b) t=33 s (T_{max}=307 ℃)

(c) t=40.7 s(T_{max}=357 ℃)　(d) t=55.8 s (T_{max}=377 ℃)

(e) t=71.1 s (T_{max}=406 ℃)　(f) t=99.8 s (T_{max}=428 ℃)

图 4　搅拌摩擦焊热过程模拟结果(20 min)

Fig. 4　Simulation results of thermal process of friction stir welding

2.2　搅拌摩擦焊接头温度场分布

图 5 和图 6 分别显示的是在 $t=58$ s 时焊接区等温线俯视图以及焊接区横、纵截面等温线，从图 5 和图 6 中可见，搅拌摩擦焊焊接区的最高温度出现在距离轴肩中心二分之一到三分之二的位置，虽然轴肩边缘具有最大的线速度和速度梯度，但整个焊接区最高温度并不出现在轴肩边缘，这是因为轴肩边缘虽然是产热最大的区域，但同时也向周围材料散热，而只有轴肩二分之一到三分之二处，由于产热大而散热差，热量积累造成这里的焊接温度最高. 从焊接区的横截面和纵截面可以看出，焊接区前端的温度梯度要大于焊缝后端的温度梯度，焊接区上部的温度梯度要大于焊缝底端的温度梯度. 这表明在搅拌摩擦焊焊接区中，热量的产生主要依靠轴肩的摩擦挤压变形作用. 从实际焊缝来看，焊缝的上端和前端受搅拌头挤压的作用，其应力和应变程度都比较高，由于在搅拌摩擦焊的稳定焊接阶段，系统的产热主要是材料的变形产热，因此在焊接区的前端和上端温度比较高，形成的温度梯度也比较大.

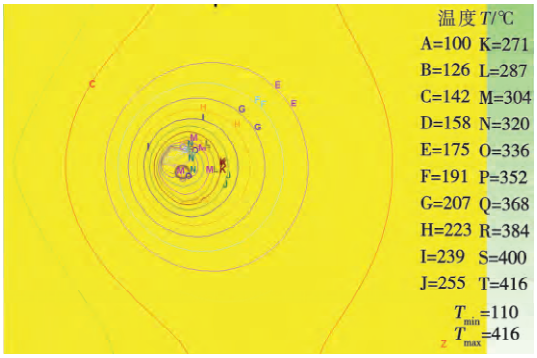

图 5　焊缝的等温线俯视图(t=58 s)

Fig. 5　Top view of isotherm of weld

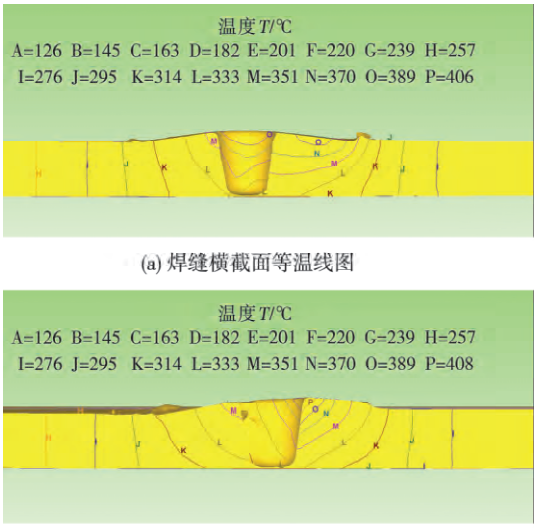

(a) 焊缝横截面等温线图

(b) 焊缝纵截面等温线图

图 6　焊缝纵、横截面的温度场分布(t=58 s)

Fig. 6　Distribution of temperature field of longitudinal and transverse section of weld

图 7 显示的是在 $t = 85$ s 时焊接区横截面上不同位置的温度分布，图 7 中 x 轴即图 3 的 x 轴. 从图 7 中可以看出，焊接区上表面的温度最高，随着深度增加，温度逐渐降低，出现这样的分布情况是因为在焊缝的上表面轴肩与铝板摩擦产生热量，此处搅拌头轴肩与铝板接触的区域作为一个整体热源，体积相对较大，远超搅拌针与铝板接触区域的体积，因此由粘滞耗散产生的热量也较多，远高于搅拌针产生的热量，所以上部的温度最高，并且最高温度出现在轴肩影响区约二分之一半径的位置，这与之前的预测相同.

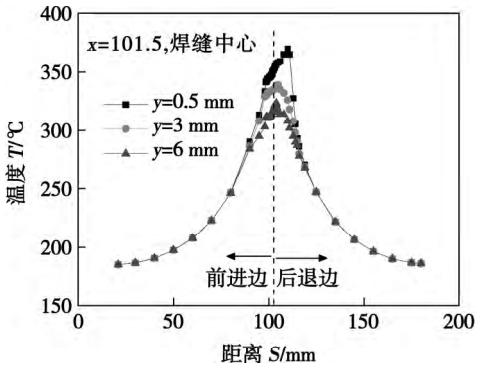

图 7 焊缝横截面不同位置的温度分布

Fig. 7 Temperature distribution of different locations of transverse section of weld

观察焊接区界面上的温度分布还可以发现，焊接区上的最高温度随着沿焊缝向底端方向移动，其最高值由偏离焊缝中心二分之一半径的位置逐渐向焊缝中心位置回归，这是因为焊缝中某处的内能受热传导和产热两方面的因素决定，其大小受输入和输出热量的多少而决定，对于焊缝中的某点来说，输入的热量包括产热和之前的热传导传输的热量，而输出的热量则主要是该处通过热传导传输出的热量. 分析焊缝中的产热截面，随着焊接区向底端方向移动，焊接区受上表面产热源热传导过来的热量影响越来越小，而主要受搅拌针产热的影响，而搅拌针周围的产热主要受到搅拌针周围金属的塑性变形产热的影响，因此最高温度在焊缝的中下部向搅拌针的中心位置回归.

在距离焊缝中心约 ±20 mm 以外的位置，搅拌头的热影响区达到一个相对平衡的状态，即铝板体内的温度保持一个相同的温度，而在焊缝中心 ±20 mm 以内的位置，受到搅拌头轴肩和搅拌针产热的影响，在该区域内的厚度方向上材料存在着温度梯度，这易导致焊接区中材料的流动和扩散等运动，由于铝合金的热影响区定义为经历了一个温度升高到 250 ℃以上的等效热处理状态的区域，从图 7 中也可以看出，距离焊缝中心约 ±20 mm 以内的区域属于焊缝的外缘至热影响区边缘的位置. 其中焊缝上表面的温度整体比焊缝底端的温度高约 30 ~ 45 ℃，后退边的温度比前进边的温度高约 20 ℃.

为验证模拟结果，采用热电偶对搅拌摩擦焊过程温度场进行实际测定. 为测定同一时刻焊缝横截面不同深度上的温度，在预设相同的试验条件下测量了三对试片，分别测量距离上表面 0.5，3 和 6 mm 位置的温度. 图 8 显示的是在搅拌头焊接至 $t = 85$ s 时刻，焊缝横截面不同深度上横向温度分布情况，x 轴即图 3 的 x 轴. 由于实际装配条件、环境温度、测量误差等影响，实际测量的数值相较于模拟温度在焊接区域有所差异，但温度场分布形状和趋势是大致相符的，并且模拟偏差在 10% 以内，证明了该数据模型的准确性.

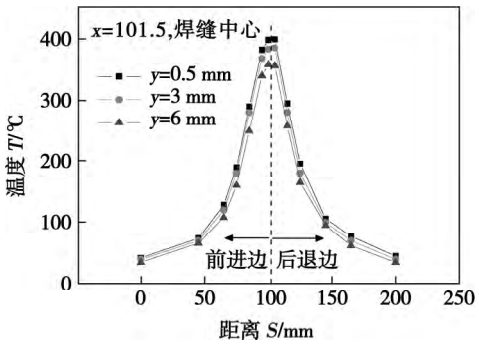

图 8 $t = 85$ s 时刻焊缝横截面不同位置实际温度分布

Fig. 8 Temperature distribution of different locations of transverse section of real weld

3 结 论

(1) 在稳定焊接阶段，受搅拌针和轴肩热力作用的影响，搅拌针作用区域的温度梯度呈现上密下疏、前密后疏的分布状态.

(2) 搅拌摩擦焊焊缝的最高温度出现在搅拌头前端偏向后退侧的搅拌针与轴肩的过渡区，焊缝后退边的温度要高于前进边的温度约 20 ℃；焊缝上下表面的温差在 30 ~ 45 ℃.

(3) 搅拌针底部的温度可达到 350 ℃以上，超过 2219 铝合金的再结晶温度，该温度可确保搅拌摩擦焊焊缝根部组织的相互扩散再结晶，形成紧密的焊缝.

[下转第 70 页]

的BGA焊点检测算法[J]. 焊接学报, 2011, 33(4): 13-16.
Zhang Ruiqiu, Zhang Xianmin, Chen Zhong, *et al*. BGA solder joint inspection algorithm based on 3D X-ray and Fisher criterion [J]. Transactions of the China Welding Institution, 2011, 33(4): 13-16.

[3] 王 欢, 杨 平, 谢方伟, 等. 复合加载下焊点寿命的数值模拟[J]. 焊接学报, 2012, 33(12): 65-68.
Wang Huan, Yang Ping, Xie Fangwei, *et al*. Study on life-prediction of solder joint under combined loading [J]. Transactions of the China Welding Institution, 2012, 33(12): 65-68.

[4] 陈 颖, 康 锐. 球栅阵列封装焊点寿命预测的综合方法[J]. 焊接学报, 2009, 30(11): 105-108.
Chen Ying, Kang Rui. Integrated life prediction method of ball grid array soldered joint [J]. Transactions of the China Welding Institution, 2009, 30(11): 105-108.

[5] Hofmeister J P, Lall P, Russ Graves. In-situ, real-time detector for faults in solder joint networks belonging to operational, fully programmed field programmable gate arrays (FPGAs) [C] // 2006 IEEE Autotestcon Conference, Anaheim, USA, 2006: 237-243.

[6] Hofmeister J P, Lall P, Goodman D, *et al*. Intermittency detection and mitigation in ball grid array (BGA) packages [C] // 2007 IEEE Autotestcon Conference, Baltimore, USA, 2007: 40-49.

[7] James P, Hofmeister, Pradeep Lall, *et al*. Real-time detection of solder-joint faults in operational field programmable gate arrays [C] // 2007 IEEE Aerospace Conference, Big Sky, MT, USA, 2007: 1-9.

作者简介: 王建业,男,1962年出生,博士,教授,博士研究生导师. 主要从事电子系统故障预测与健康管理方面研究. 发表论文50余篇. Email: 2216559285@qq.com

[上接第60页]

参考文献:

[1] 李敬勇, 赵阳阳, 亢晓亮. 搅拌摩擦焊过程中搅拌头温度场分布特征[J]. 焊接学报, 2014, 35(3): 66-70.
Li Jingyong, Zhao Yangyang, Kang Xiaoliang. Characteristic of temperature distributions in stirring tools during friction stir welding [J]. Transactions of the China Welding Institution, 2014, 35(3): 66-70.

[2] 鄢东洋, 史清宇, 吴爱萍. 搅拌摩擦焊接过程的试验测量及分析[J]. 焊接学报, 2010, 31(2): 67-70.
Yan Dongyang, Shi Qingyu, Wu Aiping, *et al*. Measurement and analysis of friction stir welding [J]. Transactions of the China Welding Institution, 2010, 32(2): 67-70.

[3] Khandkar M Z H, Khan J A, Reynolds A P. Predictions of temperature distribution and thermal history during friction stir welding: input torque based model [J]. Science and Technology of Welding and Joining, 2003, 8(3): 165-174.

[4] Nandan R, Roy G G, Lienert T J. Three-dimensional heat and material flow during friction stir welding of mild steel [J] Acta Materialia, 2007, 55: 883-895.

[5] 赵衍华, 林三宝, 贺紫秋, 等. 铝合金搅拌摩擦焊接过程数值模拟[J]. 机械工程学报, 2006, 42(7): 92-97.
Zhao Yanhua, Lin Sanbao, He Ziqiu, *et al*. Numerical simulation of 2014 aluminium alloy friction stir welding process [J]. Chinese Journal of Mechanical Engineering, 2006, 42(7): 92-97.

[6] 张洪武, 张 照, 陈金涛, 等. 搅拌摩擦焊接过程的有限元模拟[J]. 焊接学报, 2005, 26(9): 13-18.
Zhang Hongwu, Zhang Zhao, Chen Jintao, *et al*. Finite element analysis of friction stir welding process [J]. Transactions of the China Welding Institution, 2005, 26(9): 13-18.

作者简介: 杜岩峰,男,1977年出生,博士,高级工程师. 主要从事先进焊接技术研究和工程应用工作. 发表论文3篇,申报国防专利2项,获国防科技进步二等奖1项. Email: duyanfeng2000@hotmail.com

method data, the turning point of S－N curve requires turning transition. In order to make the S－N curve and the breaking point N_0 have more engineering application value, the theory and method of transition point connected with variable slope curve was proposed. The feasibility of using variable slope method has been verified by experiment, and the two curves were compared by analysis . The results show that the new method of drawing the S－N curve can display the performance of welding joints spot more accurately.

Key words: spot welded joints; S－N curve; breaking point N_0; variable slope slash transition

Analysis of vibration fatigue S－N curve on Q235B steel butt welded joint FAN Wenxue[1,2], CHEN Furong[1], XIE Ruijun[1], TANG Dafu[1] (1. Institute of Materials Science and Engineering, Inner Mongolia University of Technology, Hohhot 010051, China; 2. Mining Institute, Inner Mongolia University of Technology, Hohhot 010051, China). pp 39－42

Abstract: The interrelation of static fatigue S－N curve and vibration fatigue S－N curve on Q235B steel butt welded joints has been analyzed. The result shows they have the same slope, and vibration fatigue S－N curve is a continuous curve without horizontal section. It moves a specified distance in stress axis. At the same time, the vibration fatigue S－N curve expression was input. In this paper, the static fatigue test and tensile test under different load frequency were done. And vibration fatigue correction factor was 0.345 2. Through correction of residual stress and size, the fatigue limit was 114.84 MPa when the cycles were 5×10^6 under vibration fatigue S－N curve. And it only has a little bias 7.60%, it shows that the method of this paper can be used to infer vibration fatigue S－N curve of Q235B steel.

Key words: Q235B steel welded joint; vibration fatigue; S－N curve

Formation process of hot cracking in copper He shielding gas tungsten welding LI Yinan[1], YAN Jiuchun[2], GUO Feng[1], PENG Zilong[1] (1. Department of Mechanical Engineering, Qingdao Technological University, Qingdao 266033, China; 2. State Key Laboratory of Advanced Welding Production Technology, Harbin Institute of Technology, Harbin 150001, China). pp 43－47

Abstract: The formation mechanism of hot cracking in gas tungsten arc welding (GTAW) of copper structures in large dimensions was researched. The dynamic formation process of hot cracking was observed and analyzed. The formation criterion of hot cracking was optimized based on the Prokhorov's theory, and the finite element model of thick copper plates in GTA welding was established based on the rigid restraint cracking test. It is concluded that the internal deformation rate $\Delta\varepsilon$ is the internal reason of forming hot cracking. The variation of the transverse tensile stress and the $\Delta\varepsilon$ in brittle temperature range (BTR) was obtained. And the formation mechanism of hot cracking without preheating was carried out compared $\Delta\varepsilon$ with high temperature ductility of HS201 welded metal. The variation of $\Delta\varepsilon$ in difference preheating temperature was analyzed to prevent hot cracking forming, and it can be concluded that the $\Delta\varepsilon$ in BTR could be declined by preheating process and the cracking susceptibility will be decreased.

Key words: copper; hot cracking; gas tungsten arc welding

Modeling and control of the nonlinear joints system of mobile repair welding robot LIU Jiajun[1], SUN Zhenguo[1], ZHANG Wenzeng[1], CHEN Qiang[1,2] (1. Key Laboratory for Advanced Materials Processing Technology, Department of Mechanical Engineering, Tsinghua University, Ministry of Education, Beijing 100084, China; 2. Yangtze Delta Region Institute of Tsinghua University, Jiaxing 314006, China). pp 48－52

Abstract: Highly nonlinear units such as deadzone and backlash exist in the joints of mobile repair welding robot, which have negative effects on control accuracy. To improve the path control accuracy of the end effector, Particle swarm optimization algorithm is used to identify the model of the nonlinear joints system. Then switching compensation control method referring the identified model is applied to the joint controlling system, combined with feedfoward-feedback control based on inverse kinematics, the hybrid control method realize considerable path accuracy. Experiments show that the average path error of designed welding robot's end effector is less than 0.2 mm with this control method, and the shortcomings of low precision reducer are compensated.

Key words: mobile welding robot; nonlinear system; identification; backlash compensation; feedforward

Feature characters extraction with visual attention method based on three-light-path weld pool images ZHANG Yan, LÜ Na, HUANG Yiming, CHEN Shanben (Intelligentized Robotic Welding Technology Laboratory, Shanghai Jiaotong University, Shanghai 200240, China). pp 53－56

Abstract: Seam tracking and weld penetration control are key parts of weld quality control. A three-light-path vision sensing system is used in the experiments to obtain the images of the top-front, top-back and back paths of the weld pool during the Al alloy GTAW welding and project them in the same picture at the same time. The image contains information of the seam, weld pool and back weld pool. The method of visual attention is adopted to find the small areas related to weld pool feature characters, and extract these characters from the image. The results show that, in real-time detection of the weld pool features during the welding process, the method of visual attention is more clarified and efficient than general methods as it focuses only on interested small areas.

Key words: welding quality control; weld pool image processing; visual attention; region of interest detection

Investigation on three-dimensional real coupling numerical simulation of temperature field of friction stir welding of 2219 aluminum alloy DU Yanfeng[1,2], BAI Jingbin[1], TIAN Zhijie[1], LI Jinsong[1], ZHANG Yanhua[2] (1. Capital Aerospace

Machinery Company, Beijing 100076, China; 2. School of Mechanical Engineering and Automation, Beijing University of Aeronautics & Astronautics, Beijing 100191, China). pp 57 – 60, 70

Abstract: To make the complicated process of heat and force of friction stir welding to be simulated more close to the actual state, we established the three-dimension mathematical model of stirring friction welding process, and analyzed thermal process and temperature field distribution of friction stir welding of 2219 aluminum alloy by means of the finite element method with 3D coupled model. Numerical simulation results show that, the temperature gradient of weld is different which the upper side is more compact than lower side and the advanced side is more compact than back side. The highest temperature is located at the transition zone of the back side between the stir-pin and the stir-head shoulder, the temperatures on the retreating side is higher than that on the advancing side, and it will be assured of tight weld if the temperatures of the area on the bottom of stir-pin are in excess of the recrystallization temperature of 2219 aluminum alloy when welding. At last, the result will provide a support for based research and technology optimization of friction stir welding.

Key words: 2219 aluminum alloy; friction stir welding; thermal process; numerical simulation

Variations of the microstructure and mechanical properties for the thick aluminum friction stir welding joint along the thickness direction GAO Hui[1], DONG Jihong[2,3], ZHANG Kun[3], LUAN Guohong[3] (1. Beijing Institute of Petrochemical Technology, Beijing 102617, China; 2. Mechanical and Electrical Engineering College, Beijing University of Chemical Engineering, Beijing 100029, China; 3. Beijing Aeronautical Manufacturing Technology Research Institute, Aviation Industry Corporation of China, Beijing 100024, China). pp 61 – 65

Abstract: Through the hierarchical method, microstructure and mechanical properties in different areas of the weld nugget zone for 30 mm thick 7A05-T6 aluminum alloy friction stir welding join have been studied. The results show that, the size of recrystallization grain in the near area of surface is largest. When the rotation speed is 360 r/min and the welding speed is 100 mm/min, for the area of T_1 to T_5, the tensile strength separately is 326, 354, 342, 334 and 307 MPa, the yield strength and elongation are also increased gradually. The fracture micrographs show that, there are a lot of mesh dimples in the fracture surface, and they are deeper on slicing T_2 especially. The hardness profile is not central symmetric, and hardness value of top area is larger than that of lower area. Friction heat will decrease with the increase of thickness, and that is the reason why the performance decline at the middle and bottom of workpiece joint.

Key words: friction stir welding; mechanical properties; microstructure; 7A05-T6 aluminum alloy

Research on the fault diagnosis technology of connection failure belonging to the FPGA solder joint WANG Jianye, DING Hao, LIU Cang, LIANG Qinglong (Air and Missile Defense Academy of Air Force Engineering University, Xi'an 710051, China). pp 66 – 70

Abstract: This paper presents a model for detecting faults in FPGA (field programmable gate array) devices of BGA (ball grid array) type of packages using the method of SJ BIST (solder joint built-in self-test). It was theoretical analyzed in details, and simulated by simulation software – multisim. The DE2 hardware system of the Altera corporation was used to verify the model. The results showed that, compared with reference, the method of SJ BIST was analyzed in more detail, and the accurate impedance could be determined more accurately, and more exact information about health state of the FPGA solder joints can be obtained.

Key words: solder joint built-in self-test; field programmable gate array; ball grid array; solder joint; fault diagnosis

Experimental research on electron beam welding of titanium alloy to stainless steel based on Cu/V filler metals with different shapes WANG Ting[1], ZHANG Binggang[2], ZHANG Yanqiao, FENG Jicai[1,2], ZHONG Shisheng[3] (1. Shandong Provincial Key Laboratory of Special Welding Technology, Harbin Institute of Technology at Weihai, Weihai 264209, China; 2. State Key Laboratory of Advanced Welding and Joining, Harbin Institute of Technology, Harbin 150001, China; 3. School of Mechatronics Engineering, Harbin Institute of Technology, Harbin 150001, China). pp 71 – 74

Abstract: Electron beam welding experiments of TA15 titanium alloy to 304 stainless steel using Cu/V filler metals with different shapes were carried out in present paper. Microstructure and mechanical properties of welding joints were examined. The results showed that the weld with lamellar structure Cu/V filler metal was characterized by solid solutions of vanadium, copper and iron. But an incomplete fusion defect was detected in bottom weld for the unmelted vanadium layer. The tensile strength was 288 MPa. When a wedge-shaped filler metal was used, microstructure remained the transition of various solid solutions. Meanwhile, the incomplete fusion defect was eliminated. Tensile strength reached 385 MPa, up to 75% of that of stainless steel. The weld zone with unmelted vanadium layer was the weakest part of the joint and facture occurred in this region in the joints welded with Cu/V filler metal with different shapes.

Key words: TA15 titanium alloy; 304 stainless steel; electron beam weldng; shape of filler metal; microstructure; mechanical properties

Research on unified adjustment of pulsed MIG welding parameters based on least squares method XUE Jiaxiang[1], JIANG Chengfeng[1], ZHANG Xiaoli[1,2], ZHU Xiaojun[1], ZHU Qiang[1] (1. Shool of Mechanical and Automotive Engineering, South China University of Technology, Guangzhou 510640, China; 2. College of Mechanical and Electrical Engineering, Jiangxi University of Science and Technology, Ganzhou 341000, China)). pp 75 – 78

Abstract: In view of the sophisticated welding parameters of digital welding machine, large-scale technology experiments